JOURNAL OF Materials CHEMISTRY

Preparation of Fe–Mo–C ternary carbide by mechanical alloying

J. J. Zhu,[a,c] Jianzhong Jiang,*[a] C. J. H. Jacobsen[b] and X. P. Lin[c]

[a]*Department of Physics, Building 307, Technical University of Denmark, Lyngby DK-2800, Denmark. E-mail: jiang@fysik.dtu.dk*
[b]*Haldor Topsøe A/S, Nymøllevej 55, Lyngby DK-2800, Denmark*
[c]*Key Laboratory of Fine-Chemical Engineering, Jiangsu Institute of Petro-Chemical Technology, Changzhou 213016, P.R. China*

Received 17th October 2000, Accepted 27th November 2000
First published as an Advance Article on the web 29th January 2001

The ternary carbide η-Fe_3Mo_3C was synthesized by mechanical alloying of elemental Fe, Mo, and graphite and subsequent heat treatment. The alloying process in the Fe–Mo–C system and the thermal stability of the ball-milled sample have been studied by X-ray powder diffraction and Mössbauer spectroscopy. It is found that alloying occurs in the Fe–Mo–C system during ball-milling. Initially, the milling process reduces the grain sizes of the pure elements and Fe–C alloying occurs to form an amorphous Fe_3C-type phase. With increasing milling times, Mo diffuses into the Fe–C alloys, which accelerates the formation of the non-magnetic amorphous Mo–Fe–C alloy. The content of Mo in the amorphous Mo–Fe–C alloy increases with milling time. After 60 to 90 hours ball-milling, a crystallization reaction of the amorphous Mo–Fe–C alloy into η-Fe_3Mo_3C and Mo_2C occurs. The ball-milled samples are composed of η-Fe_3Mo_3C, Mo_2C, and residual amorphous Mo–Fe–C alloy together with a slight contamination from the WC balls. It is found that the reaction between Mo_2C and the residual amorphous Mo–Fe–C phase occurs at low temperatures while WC reacts with η-Fe_3Mo_3C to form Fe_3W_3C at high temperatures. The samples annealed at high temperatures (>1073 K) are composed of crystalline η-Fe_3Mo_3C-type phases (η-Fe_3Mo_3C with an isomorphous substitution of W for Mo) with a lattice constant of 11.117(8) Å and an isomer shift of $-0.21(1)$ mm s^{-1}.

1. Introduction

Ternary carbides are a class of solid-state materials which have received considerable attention from the materials community. Three of the factors responsible for this interest are: (1) the higher order carbide compounds are expected to display different, more complex, crystal structures and more exotic magnetic, optical and electrical properties than their binary counterparts; (2) to date, the preparation of ternary carbides using traditional approaches has proven to be quite challenging and may require the development of new synthetic strategies, which could eventually be used in the development of other new compounds; (3) their potential applications in fields such as catalysis,[1–6] magnetic materials,[7] and cutting tools. Unfortunately, there has been little work with ternary carbides up to now.[7–10] Although ternary carbides can be synthesised *via* high temperature methods or temperature-programmed reactions, the success of the synthesis depends on the choice of the carburisation gas composition.[11] In addition, the deposition of amorphous or graphitic carbon on the surface of the carbides during carburisation is another difficulty.[11]

More than 20 years ago, mechanical alloying was developed as a way of circumventing the limitations of conventional alloying. Since the discovery by Koch *et al.*,[12] demonstrating that amorphous $Nb_{40}Ni_{60}$ can be formed by the mechanical alloying of elemental powder blends, mechanical alloying has emerged as a versatile technique for the production of materials far from equilibrium in a variety of systems, for example, amorphous alloys, nanostructured alloys, and metastable solid solutions.[13–16] In this metallurgical process, powder particles are subjected to severe mechanical deformation during collisions with balls and the vial, and are repeatedly deformed, cold welded, and fractured, so that solid-state reaction and/or mechanochemical reaction can be facilitated in powder blends. Although the principles governing these reactions are, in many cases, incompletely understood and are also undoubtedly system specific, the formation of many compounds prepared by mechanochemical reaction, for example, borides,[17] nitrides and carbides,[8,18–24] and silicides,[25,26] have been reported in the literature. However, relatively few studies on the synthesis of ternary carbides have been published.[8] In this work, mechanical alloying in the prototypical ternary carbide system, Fe_3Mo_3C, has been investigated. The microstructural changes occurring during mechanochemical reactions and heat treatments in the Fe–Mo–C system were monitored by X-ray powder diffraction (XRD) and Mössbauer spectroscopy.

2. Experimental

Ball-milling experiments were performed using a planetary ball-mill (Fritsch Pulverisette 5). The device consisted of nine tungsten carbide balls with 20 mm diameter confined in a horizontal tungsten carbide cylinder vial (75 mm inner diameter, 250 ml volume). Powders of iron (purity > 99.5%, Fluka), molybdenum (purity > 99.9%; 200 mesh; Alfa) and graphite (purity > 99.0%; > 300 mesh; Alfa) with a stoichiometric composition of 3Fe : 3Mo : 1C were mixed and sealed under argon. The milling speed was set at 200 rotations per minute with a ball-to-powder weight ratio of 19 : 1. Small samples of the powder were removed from the vial for analysis at different milling intervals, such as 0.5, 5, 10, 20, 40, 60, and 90 hours. The samples corresponding to different ball-milling times were labelled as F05, F5, F10, F20, F40, F60 and F90, respectively. Heat treatments of sample F90 were performed in a quartz tube under an argon atmosphere (purity, 99.999%) at 673, 773, 873, 973, 1073, 1173, and 1273 K for one hour.

The Mössbauer spectra were recorded at 295 and 20 K by employing a standard transmission Mössbauer spectrometer and a ^{57}Fe source. The spectrometer was calibrated using a

 DOI: 10.1039/b008365h

standard α-Fe foil at 295 K and the isomer shifts were given relative to α-Fe at 295 K. For low temperature measurements, a closed-cycle helium cryostat was used. A home-written program (as described in our previous work) was used to fit the Mössbauer spectra.[27] In the fitting process, all Mössbauer parameters are free and small values of χ^2 were obtained for all spectra. X-Ray powder diffraction patterns were taken at room temperature by means of a Philips vertical powder diffractometer using Cu-Kα radiation ($\lambda = 1.54178$ Å). The composition of sample F90 was determined by inductively coupled plasma spectroscopy (ICP). It was found that the tungsten contamination was less than 5 wt% together with Fe : Mo ≈ 1 : 1.

3. Results and discussion

3.1. Alloying process

Fig. 1 shows the X-ray powder diffraction patterns of the mixture of Fe, Mo and graphite powders with different ball-milling times. For the sample milled for 0.5 hours, the X-ray powder diffraction pattern shows diffraction peaks from the pure elements: iron, molybdenum and graphite. After 5 hours ball-milling, the increased peak widths for Fe and Mo indicate a reduction in grain size and/or an increase in strain in the sample. The Bragg peak of graphite disappears. For a ball-milling time of 10 hours, the Bragg peaks of Fe and Mo are broadened and the background is enhanced. After 20 hours, an amorphous phase appears at $2\theta \approx 42^\circ$, while the Bragg peaks of Fe disappear and WC, a product of contamination from the vial and milling balls, is detected. Omuro *et al* has performed detailed investigations on the effect of Mo on the formation of the amorphous phase during the mechanical alloying process in the Fe–C system.[9] It was found that a small amount of Mo (3 at%) could accelerate the formation of amorphous Mo-doped Fe–C alloy. Thus, the amorphous phase observed here may also be due to the Mo-doped Fe–C alloy. For a milling time of 40 hours, the relative intensity of the amorphous phase further increases, while the Bragg peaks of Mo and WC can still be seen. After 60 hours ball-milling, new peaks are observed, corresponding to η-Fe_3Mo_3C and Mo_2C, whereas the Mo diffraction peaks disappear. This means that the Mo-doped Fe–C amorphous phase is partially crystallized into η-Fe_3Mo_3C and Mo_2C phases. In the final stage, after 90 hours ball-milling, the XRD pattern can be assigned to η-Fe_3Mo_3C, residual amorphous Mo–Fe–C alloy, Mo_2C, and WC.

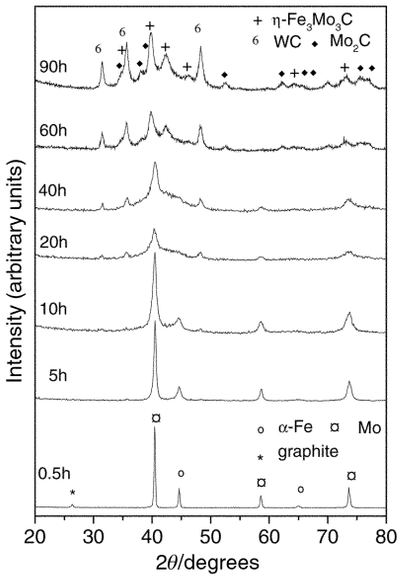

Fig. 1 X-Ray powder diffraction patterns of the mixture of Fe, Mo, and C powders after various ball-milling times.

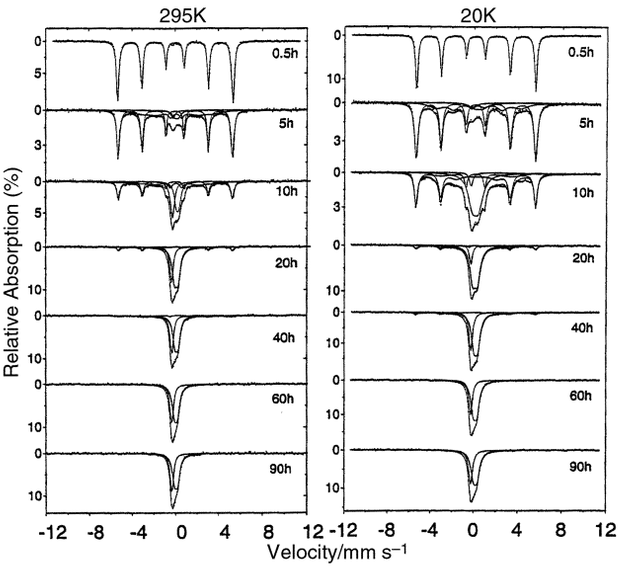

Fig. 2 Mössbauer spectra recorded at 295 and 20 K for the mixture of Fe, Mo, and C powders after various ball-milling times.

The Mössbauer spectra recorded at 295 and 20 K for samples with various milling times are shown in Fig. 2. The data points are difficult to see because they are almost completely overlapped by the solid lines of the fits. The hyperfine parameters obtained from fitting the spectra of the samples are listed in Tables 1 and 2. For a milling time of 0.5 hours, the Mössbauer spectrum is identical to that of α-Fe with a hyperfine field of 33 T. After 5 hours milling, the spectrum can be fitted with a broadened sextet (19.6 T and 31.1%), a doublet (6.3%) and a singlet (3%) together with the bcc-Fe sextet (59%). On the basis of the Mössbauer parameters,[23,28,29] the broadened sextet could be attributed to an amorphous Fe_3C-type phase while the doublet and singlet might be due to the Mo-doped Fe–C amorphous phase. It should be mentioned that the Mo-doped Fe–C amorphous phase shows a broadened non-symmetrical paramagnetic spectrum, which should be fitted with a distribution of Mössbauer parameters, corresponding to various local atomic environments. Here we used only one doublet and one singlet to fit the spectrum. Furthermore, the singlet is also superimposed onto the pure Fe_3Mo_3C component (details given later). The results indicate that solid reactions occur after only 5 hours of milling. Note that the amorphous Fe_3C-type phase was not detected by XRD measurements, which might be due to the amorphous structure of the phase. With increasing ball-milling time, the non-magnetic component increases at the expense of the magnetic component. Fig. 3 shows the relative

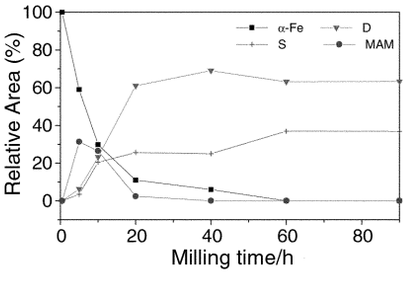

Fig. 3 Relative areas of different components obtained from the Mössbauer spectra for the mixture of Fe, Mo, and C powders after various ball-milling times. S, D, and MAM denote the singlet, the doublet, and the magnetic amorphous Fe_3C-type phase, respectively. The lines are guides to the eye.

Table 1 Mössbauer parameters at 295 K, hyperfine fields (H), isomer shifts (IS) with respect to α-Fe, quadrupole splitting (QS), line width (Γ) of the outer lines in sextets and relative resonance area (RA) for the mixture of Fe, Mo, and C powders after various ball-milling times

Time/h	Component[a]	H/T	IS/mm s^{-1}	QS/mm s^{-1}	Γ/mm s^{-1}	RA (%)
0.5	α-Fe-type component	32.9	0	0	0.29	100
5	α-Fe-type component	32.6	0	0	0.30	59.0
	MAM	19.6	0.09	−0.02	2.34	31.3
	D	—	0.14	0.36	0.51	6.3
	S	—	−0.19	—	0.41	3.4
10	α-Fe-type component	32.6	0.01	0	0.34	29.8
	MAM	20.7	−0.09	−0.18	3.0	26.5
	D	—	0.24	0.26	0.44	23.2
	S	—	−0.25	—	0.44	20.5
20	α-Fe-type component	32.6	0.02	0	0.36	11.0
	MAM	21.2	0.01	0	0.41	2.4
	D	—	0.10	0.35	0.48	61.0
	S	—	−0.33	—	0.34	25.6
40	α-Fe-type component	31.5	−0.03	−0.01	0.88	8.2
	D	—	0.08	0.36	0.46	67.5
	S	—	−0.34	—	0.32	24.3
60	D	—	0.06	0.29	0.48	63.1
	S	—	−0.32	—	0.38	36.9
90	D	—	0.07	0.30	0.46	63.2
	S	—	−0.32	—	0.35	36.8

[a]D: The doublet component in the non-magnetic Mo–Fe–C amorphous phase. S: The singlet component in the non-magnetic Mo–Fe–C amorphous phase. MAM: Magnetic amorphous Fe_3C-type alloy.

areas of various components as a function of milling time. After 60 h, no magnetic component was detected and the spectrum is composed of one doublet and one singlet. In the final stage, 90 hours milling, the spectrum is almost the same as that of the sample milled for 60 hours. By comparing the spectra recorded at 295 K with those recorded at 20 K, no obvious difference was observed, indicating that the superparamagnetic effect, which is caused by the reduction in grain size of the magnetic particles during ball milling, on the non-magnetic doublet and singlet is most likely negligible. From the non-magnetic component for samples milled from 10 to 90 h and the corresponding XRD patterns, it can be concluded that the Mössbauer spectrum for η-Fe_3Mo_3C is superimposed onto that of the Mo–Fe–C amorphous alloy.

3.2. Thermal stability

To investigate the crystallization process for the ball-milled samples, F90 was annealed in an argon flow at 673, 773, 873, 973, 1073, 1173 and 1273 K for one hour. Fig. 4 shows the XRD patterns recorded from the samples annealed at various temperatures. After annealing at 673 and 773 K, the Bragg peaks become slightly narrower compared to the as-milled sample. This suggests that low temperature heat treatments result in stress release and grain growth. At 873 K, the residual amorphous phase almost disappears, as estimated from the fitting results of the Bragg peaks and baseline in the 2θ range from 25 to 55°. The peaks for Mo_2C become weak while the intensities of the peaks for η-Fe_3Mo_3C increase, indicating that Mo_2C reacted with the residual amorphous phase to form η-Fe_3Mo_3C. Above 973 K, the Mo_2C diffraction peaks disappear. After annealing at 1073 K, the intensities of peaks for WC decrease dramatically while no new diffraction peaks are observed. It is known that Fe_3W_3C and η-Fe_3Mo_3C are isostructural with lattice parameters of 11.087 and 11.1355(10) Å, respectively.[30] Thus, it is reasonable to suggest that Fe_3W_3C is formed by the reaction between WC and η-Fe_3Mo_3C at high temperatures. In the XRD pattern of the

Table 2 Mössbauer parameters at 20 K, hyperfine fields (H), isomer shifts (IS) with respect to α-Fe, quadrupole splitting (QS), line width (Γ) of the outer lines in sextets and relative resonance area (RA) for the mixture of Fe, Mo, and C powders after various ball-milling times

Time/h	Component[a]	H/T	IS/mm s^{-1}	QS/mm s^{-1}	Γ/mm s^{-1}	RA (%)
0.5	α-Fe-type component	33.7	0.12	0	0.27	100
5	α-Fe-type component	33.8	0.12	0	0.40	64.0
	MAM	23.7	0.32	0.02	1.65	25.0
	D	—	0.38	0.72	1.03	7.3
	S	—	0.23	—	0.83	3.8
10	α-Fe-type component	33.9	0.13	0	0.37	31.9
	MAM	19.7	0.15	0.03	0.44	28.1
	D	—	0.16	0.57	0.95	36.8
	S	—	0.25	—	0.36	3.2
20	α-Fe-type component	33.8	0.14	0.02	0.45	11.8
	MAM	19.7	0.11	0	0.47	8.9
	D	—	0.14	0.43	0.60	68.9
	S	—	0.24	—	0.31	10.5
40	α-Fe-type component	33.9	0.12	0.01	0.51	7.7
	D	—	0.24	0.34	0.55	63.8
	S	—	0.23	—	0.39	28.5
60	D	—	0.18	0.33	0.54	69.2
	S	—	0.23	—	0.39	30.8
90	D	—	0.20	0.33	0.56	64.4
	S	—	0.22	—	0.43	35.6

[a]D: The doublet component in the non-magnetic Mo–Fe–C amorphous phase. S: The singlet component in the non-magnetic Mo–Fe–C amorphous phase. MAM: Magnetic amorphous Fe_3C-type alloy.

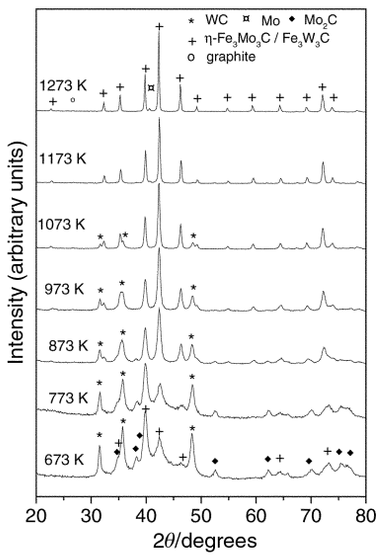

Fig. 4 X-Ray powder diffraction patterns of F90 samples annealed at various temperatures for one hour.

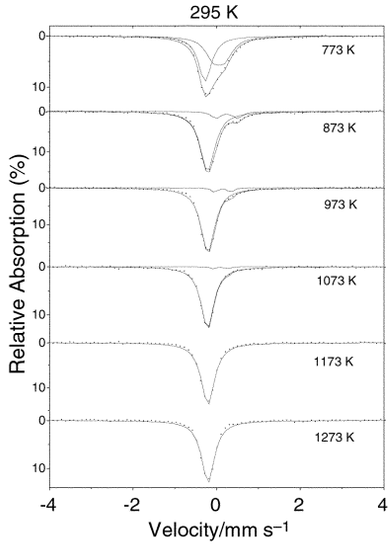

Fig. 5 Mössbauer spectra recorded at 295 K for F90 samples annealed at various temperatures for one hour.

sample annealed at 1173 K, WC diffraction peaks disappear and two tiny new peaks at $2\theta = 26.6$ and 40.5°, corresponding to graphite and molybdenum, respectively, can be detected. The formation of Mo and C further supports the suggestion, mentioned above, that WC reacts with η-Fe_3Mo_3C to form Fe_3W_3C in high temperature annealing processes. At 1273 K, the XRD pattern consists of η-Fe_3Mo_3C-type phases (η-Fe_3Mo_3C and Fe_3W_3C) with a lattice constant $a = 11.117(8)$ Å and a tiny amount of C and Mo.

Table 3 Mössbauer parameters at 295 K, isomer shifts (IS) with respect to α-Fe, quadrupole splitting (QS), line width (Γ) and relative resonance area (RA) for the F90 sample annealed at various temperatures

Temperature/K	Component	IS/mm s^{-1}	QS/mm s^{-1}	Γ/mm s^{-1}	RA (%)
773	Doublet	0.059	0.271	0.455	50.9
	Singlet	−0.275	—	0.383	49.1
873	Doublet	0.142	0.515	0.279	12.5
	Singlet	−0.215	—	0.422	87.5
973	Doublet	0.146	0.393	0.150	5.0
	Singlet	−0.209	—	0.400	95.0
1073	Doublet	0.094	0.344	0.150	2.5
	Singlet	−0.218	—	0.371	97.5
1173	Singlet	−0.207	—	0.389	100
1273	Singlet	−0.205	—	0.372	100

Fig. 5 shows the Mössbauer spectra recorded at 295 K for the samples annealed at various temperatures. The spectra were fitted with only one singlet or one doublet and one singlet. Mössbauer parameters are listed in Table 3. With increasing annealing temperature, the relative area of the singlet increases while that of the doublet decreases, indicating that the residual amorphous Mo–Fe–C phase becomes unstable at high temperatures. At 1173 K, only one singlet [IS = −0.21(1) mm s^{-1}] was observed. Unfortunately, it is impossible to distinguish η-Fe_3Mo_3C from Fe_3W_3C because their Mössbauer parameters are almost the same with an isomer shift of −0.2 mm s^{-1}.[31]

4. Conclusions

The mechanical alloying process in the Fe–Mo–C system and the thermal stability of the milled samples have been investigated by X-ray powder diffraction and Mössbauer spectroscopy. It is found that alloying occurs in the Fe–Mo–C system during milling. Initially, the milling process reduces the grain sizes of pure elements and Fe–C alloying occurs to form the amorphous Fe_3C-type phase. With longer milling times, Mo diffuses into the Fe–C alloys, which accelerates the formation of the non-magnetic amorphous Mo–Fe–C alloy but also increases the Mo content. After 60 and 90 hours ball-milling, a crystallization reaction of the amorphous Mo–Fe–C alloy into η-Fe_3Mo_3C and Mo_2C occurs. The samples are composed of η-Fe_3Mo_3C, Mo_2C, and residual amorphous Mo–Fe–C alloy together with the contaminant WC. It seems that the reaction between Mo_2C and the residual amorphous Mo–Fe–C phase occurs at low temperatures while WC reacts with η-Fe_3Mo_3C to form Fe_3W_3C at high temperatures. The samples annealed at high temperatures (>1073 K) are composed of crystalline η-Fe_3Mo_3C-type phases (η-Fe_3Mo_3C with an isomorphous substitution of W for Mo) with a lattice constant of 11.117(8) Å and an isomer shift of −0.21(1) mm s^{-1}.

Acknowledgements

Financial support from the Danish Technical Research Council, SINOPEC, and the Jiangsu Province Committee of Science and Technology is gratefully acknowledged.

References

1 S. T. Oyama, *Catal. Today*, 1992, **15**, 420.
2 V. L. S. Teixeira da Silva, S. Ramanathan, M. Schmal and S. T. Oyama, *Proceedings of the 8th Brazilian Congress on Catalysis.*, 1995, vol. 1, p. 420.
3 E. L. McCandlish, J. F. Wrightand L. E. Kugler, United States Patent 4,345,038, 1995.
4 E. L. McCandlishand L. E. Kuglar, United States Patent 4,337,232, 1995.
5 J.-G. Choi, J. R. Brenner, C. W. Colling, B. Demczyk and L. T. Thompson, *Symposium on Octane and Cetane Enhancement Processes for Reduced-Emissions Motor Fuels*, presented before the Division of Petroleum Chemistry, Inc., American Chemical Society, San Francisco Meeting, April 5–10, 1992.
6 L. Leclercq, M. Provost, H. Pastor, J. G. Rimblot, A. M. Hardy, L. Gengembre and G. Leclercq, *J. Catal.*, 1989, **117**, 371.
7 C. Kuhrt, *J. Magn. Magn. Mater.*, 1996, **157–158**, 235.
8 L. M. Di, A. Calka, Z. L. Li and J. S. Williams, *J. Appl. Phys.*, 1995, **78**, 4118.
9 K. Omuro, H. Miura and H. Ogawa, *Mater. Sci. Eng.*, 1994, **A181–A182**, 1281.
10 A. Machado Alves, R. Rosenthal and V. L. S. Teixeira da Silva, *Mater. Sci. Forum*, 1999, **299–300**, 121.
11 S. T. Oyama, *Catal. Today*, 1992, **15**, 179.

12 C. C. Koch, O. B. Cavin, C. G. Mckamey and J. O. Scarbrough, *Appl. Phys. Lett.*, 1983, **43**, 1017.
13 W. L. Johnson, *Prog. Mater. Sci.*, 1986, **30**, 81.
14 C. C. Koch, in *Materials Science and Technology*, editors: R. W. Cahn, P. Hassen and E. J. Kramer, vol. 15, VCH, Weinheim, Germany, 1991, p. 193.
15 J. Z. Jiang, C. Gente and R. Bormann, *Mater. Sci. Eng.*, 1998, **A242**, 268.
16 J. Z. Jiang, R. Lin, S. Mørup, K. Nielsen, F. W. Poulsen, F. J. Berry and R. Clasen, *Phys. Rev. B: Solid State*, 1997, **55**, 11; J. Z. Jiang, S. Mørup and S. Linderoth, *Mater. Sci. Forum*, 1996, **225–227**, 489.
17 L. Schultz, J. Wecker and E. Hellstern, *J. Appl. Phys.*, 1987, **61**, 3583.
18 P. Matteazi and G. Le Caër, *J. Am. Ceram. Soc.*, 1991, **74**, 1382.
19 G. Le Caër, E. Bauer-Grosse, A. Pianelli, E. Bouzy and P. Matteazzi, *J. Mater. Sci.*, 1990, **25**, 4726.
20 A. Calka and J. S. Walliams, *Mater. Sci. Forum*, 1992, **88–90**, 787.
21 W. Y. Lim, M. Hida, A. Sakakibara, Y. Takemoto and S. Yokomizo, *J. Mater. Sci.*, 1993, **28**, 3463.
22 G. M. Wang, A. Calka, S. J. Campbell and W. A. Kaczmarek, *Mater. Sci. Forum*, 1995, **179–181**, 210.
23 S. J. Campbell, G. M. Wang, A. Calka and W. A. Kaczmarek, *Mater. Sci. Eng.*, 1997, **A226–228**, 75.
24 G. M. Wang, S. J. Campbell, A. Calka and W. A. Kaczmarek, *J. Mater. Sci.*, 1997, **32**, 1461.
25 R. K. Viswanadham, S. K. Mannan and S. Kumar, *Scr. Metall.*, 1988, **22**, 1011.
26 C. G. Tschakarov and G. Gospodinov, *J. Solid State Chem.*, 1985, **59**, 265.
27 J. Z. Jiang, F. W. Poulsen and S. Mørup, *J. Mater. Res.*, 1999, **14**, 1343.
28 G. Le Caër and P. Matteazzi, *Hyperfine Interact.*, 1991, **66**, 309.
29 G. Le Caër, P. Matteazzi and E. Bauer Grosse, *J. Mater. Sci.*, 1990, **25**, 4726.
30 JCPDS cards: 06-0696, 42-1120, 75-2078, 25-1047, 77-0255, 47-1191 and 78-1990, International Centre for Diffraction Data, Swarthmore, PA, 1998.
31 B. Decaudin, C. Djega-Mariadassou and G. Cizerion, *J. Alloys Compd.*, 1995, **226**, 208.